Expert Systems With Applications 207 (2022) 118088

Contents lists available at ScienceDirect

Expert Systems With Applications

journal homepage: www.elsevier.com/locate/eswa

Review

Trajectory optimization for exposure to minimal electromagnetic pollution using genetic algorithms approach: A case study

Raúl Gallego-Martínez [a], Francisco J. Muñoz-Gutiérrez [b,1,*], Alejandro Rodríguez-Gómez [b]

[a] School of Engineering, University of Málaga, Spain
[b] Department of Electrical Engineering, School of Engineering, University of Málaga, 29071 Málaga, Spain

ARTICLE INFO

Keywords:
Electromagnetic pollution
Sustainable functionality
Electromagnetic field mapping
Trajectory planning
Genetic algorithm

ABSTRACT

Low-frequency electromagnetic pollution associated with electricity supplies and electrical appliances creates broad and specific challenges. Among them, knowing the values of this pollution in urban areas to prevent long exposure in the daily life human beings is rising in today's information society.

This paper presents a comprehensive approach for, first, mapping electromagnetic pollution of complete urban areas and, second, based on the former data, the trajectories planning of commuting with minimal electromagnetic exposure.

In the first stage, the proposed approach reduces the number of necessary measurements for the pollution mapping, estimating their value by optimizing functional criteria using genetic algorithms (GAs) and considering the superposition effect of different sources.

In the second stage, a combination of a specifically designed search space and GA as optimization algorithm makes it possible to determine an optimized trajectory that represents a balanced solution between distance and exposure to magnetic fields.

The results verify the obtaining of a complete mapping with less error, between 1% and 2.5%, in power lines and medium/low voltage (MV/LV) substations, respectively. The proposed approach obtains optimized trajectories for different types of commuting (pedestrians, bikers, and vehicles), and it can be integrated into mobile applications.

Finally, the method was tested on an actual urban area in Malaga (Spain).

1. Introduction

In today's information society, there is a wide and growing interest in knowing what factors can be decisive for the health of human beings. For this purpose, the assessment of the environmental factors, such as atmospheric, light, acoustic, and electromagnetic pollution is essential. Each of them is susceptible to the development of applications aimed at preserving public health.

In the particular case of electromagnetic pollution, the increasing electrical energy consumption due to the exponential growth of technological devices requires a dense distribution network to deliver this energy to all users. This tightly meshed installation, together with the operation of the equipment itself, produces the generation of electromagnetic fields at an industrial frequency that, in urban areas with a high population density, has given rise to an environmental problem.

This situation can worsen because there is no coordination among the responsible for the different radiation sources that, by superposition, produce the apparition of critical electromagnetic pollution points. This issue has become a problem of continuous relevance and great social interest (Nassiri, Monazzam, Hosseyni, Azam, & Shalkouhi, 2018; Paniagua, Rufo, Jiménez, & Antolín, 2020; Sturman, 2019; Tang et al., 2019).

Electromagnetic radiation at an industrial frequency generates two problems. On the one hand, electromagnetic compatibility: the malfunction in electrical or electronic equipment. On the other hand, despite being non-ionizing radiation, the related social alarm to the possible effects that an extended exposition of low pollution levels may provoke in the living beings.

There are different non-excluding options, such as radiation relief techniques (Cruz, Hoeffelman, & del Pino, 2008; del-Pino-López,

* Corresponding author.
E-mail addresses: 0610373463@uma.es (R. Gallego-Martínez), fjmg@uma.es (F.J. Muñoz-Gutiérrez), arodriguezg@uma.es (A. Rodríguez-Gómez).
[1] https://orcid.org/0000-0002-6563-4528.

https://doi.org/10.1016/j.eswa.2022.118088
Received 21 November 2021; Received in revised form 16 June 2022; Accepted 4 July 2022
Available online 8 July 2022

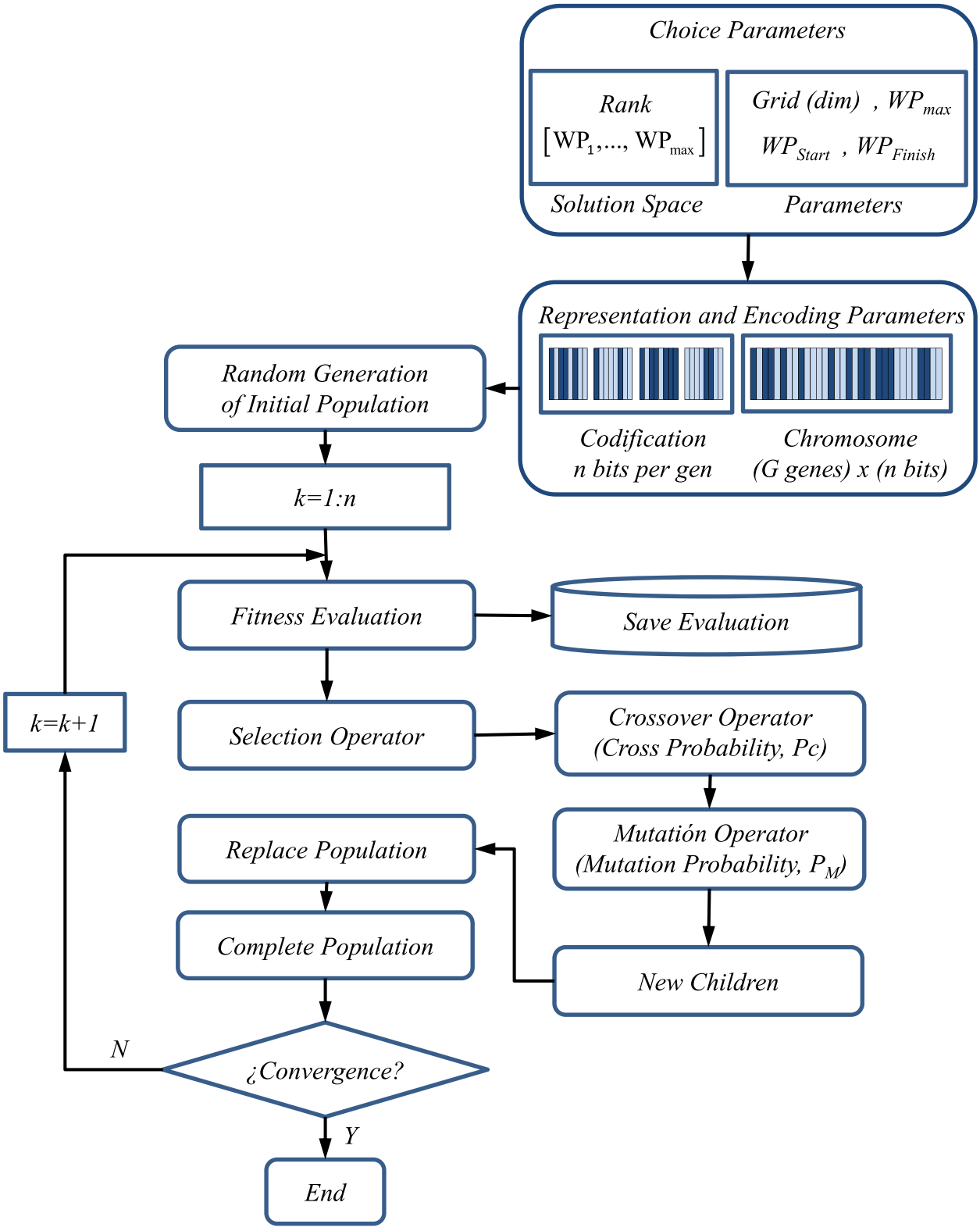

Fig. 1. Genetic algorithm flowchart.

Giaccone, Canova, & Cruz-Romero, 2015) or shielding techniques (del-Pino-López, Cruz-Romero, Serrano-Iribarnegaray, & Martínez-Román, 2014; Lucca, 2016), whose objective is to minimize electromagnetic radiation or exposition according to the limits established by the regulations (International Commission on Non-Ionizing Radiation Protection, 2010; Melnick, 2020).

Another approach, when it is not possible to reduce the emission, consists in applying mapping techniques (Filchev, Teodosiev, Nedkov, Borisova, Kehayov, Iliev, & Tsvetkov, 2019; Liu et al., 2020) for obtaining the value of the electromagnetic field at a specific point. These techniques are based on the measurement of electromagnetic radiation levels, which requires many resources, both human and material. In a

particular urban area, obtaining the necessary large-scale mapping of environmental electromagnetic radiation using conventional measurement methods would require an unaffordable amount of resources. Furthermore, in these urban areas it is not always possible to take measurements at specific points. Since it is not possible or affordable dispose all required measurements for the mapping, previous works propose to obtain these values using interpolation techniques (de Andrade et al., 2020; Sato & Fujii, 2017). Although very useful, these methods can result inaccurate for the effect of superposition of different sources.

There are alternative general-purpose models, such as the one presented in Guo, Yang, Chen, Cheng, and Gong (2019), that could be adapted to the electromagnetic mapping problem in areas with multiple sources.

In any case, the approach taken in the present work, taking advantage of the superposition principle, allows a flexible updating of the incorporation of new sources and/or modification of the existing ones.

Different alternatives, based on simulations, measurements or calculations, have been described to obtain B values generated by the medium/low voltage substations (Rathebe & Mbonane, 2018; Rozov, Pelevin, & Pielievina, 2017; Safigianni & Tsompanidou, 2009). In this regard, no previous work provides estimated values of B considering different types of generating sources.

This paper offerings a comprehensive approach for mapping electromagnetic pollution of complete urban areas that presents the following contributions:

1. It is proposed an analytical approach that reduces the number of measurements required. These empirical (measured) values are supplemented by theoretical (calculated) and estimated (algorithmic) values.
2. This approach considers the superposition effect of electromagnetic radiation generated by multiple sources at industrial frequency, considering two different kinds in urban areas: power lines (overhead or underground) and MV/LV substations.
3. It is verified that the use of GA allows obtaining estimated values with lower error than those obtained by means of interpolation techniques.

This method consists of identifying the linear and non-linear parameters of a set of functions that allow estimating the value of the electromagnetic field at a point. This value is the result of the contribution of different sources that are present in the area under study. GA identifies these functional parameters by minimizing the quadratic error between the estimated values and a subset of measured values used as a test.

On the other hand, trajectories optimization is a large field of study that began in the 60 s of the last century. In the two last decades, many applications were proposed in areas such as robotics (Kuo, Lin, & Lin, 2020; Madridano, Al-Kaff, Martín, & de la Escalera, 2021; Zhang, Dai, Zanchettin, & Villa, 2020), aviation and space flights (Asadi & Atkins, 2018; Chai, Savvaris, Tsourdos, Chai, & Xia, 2019), motor traffic (Lee, Mallipeddi, & Lee, 2017; Zhu & Aksun-Guvenc, 2020), and in multiple industrial environments (Guo et al., 2020; Long et al., 2020). The GAs were verified as an efficient tool in setting such optimal trajectories (Alijuan, Wanzhong, Xuyun, Xibo, Xin, & Baoyi, 2018; Saini, Roy, & Dogra, 2018). In any case, continuous exposure due to commuting in a polluted environment still has not been studied.

In this line, this paper presents another contribution:

4. A comprehensive approach for trajectories planning of commuting in urban areas with minimal electromagnetic exposure.

This trajectory planning is characterized by an optimal adjustment that can be modified by the user (pedestrians, cyclists, or drivers), choosing between two extremes: minimum electromagnetic contamination or minimum distance travelled, being able to choose a balanced solution between these two conditions.

For this, a specifically designed search space allows applying a GA to determine an optimized trajectory. The proposed approach is the solution of GA to a linear-quadratic problem (QL) to the sketch of optimal trajectories. The system dynamics are linear, the cost function is quadratic, and it is subjected to the constraints imposed by the accessibility conditions and traffic in the area under study.

The remainder of this paper is organized as follows. Section 2 introduces the whole approach, material, and methods. The proposed mapping technique for an area under study is described, considering power lines and MV/LV substations, and secondly, the trajectories planning. The encoding method, the crossover and the mutation mechanisms used for GAs are fully described. In Section 3, the methodology is applied to an actual urban area in Malaga (Spain), comparing results with other existing approaches. Section 4 presents the discussion of the obtained results using statistical measures. Finally, the conclusions are presented in Section 5.

2. Proposed approach

Genetic algorithm (GA) is an artificial intelligence technic used in the two principal part of the work.

The GAs are inspired in the evolutionary biological processes which combine the natural selection with the most adapted individualś survival in order to find, in an efficient way, solutions to complex problems (Fogel, Owens, & Walsh, 1966; Goldberg, 1989).

Genes, as basic elements of the GAs, are the codified values that permit getting a solution. Chromosomes are the gene arrays.

Fig. 1 shows a flowchart of the basic structure of the GAs used in the present work.

The GAs work starting from a set of codified candidate solutions (chromosomes), which satisfy a set of constraints generated randomly (initial population) upon a search space. An objective function evaluates the quality of each solution, in such a way that they are ordered from the greater adaptation to the lesser adaptation ones.

Each iteration (generation) involves three procedures (operators):

– Competitive choice of the most adapted solutions and elimination of the worst ones (selection).

– Exchange of the genetic material among the selected chromosomes to generate new solutions that substitute the eliminated ones (crossover).

– Modification through selected change of the genetic information of some chromosomes (mutation).

This iterative process allows reaching, through the operators mentioned above, in a particular search space, the desired balance between extension and intensity, avoiding voracity to optimal locals.

This process ends when the convergence criteria are reached. Setting a high value of this convergence criterion (>95%) compensates for the randomness of the initial parameterization and the variability of the different operators of the genetic algorithm.

As the population density algorithm, the last generation represents a set of ordered solutions through an adaptation value (fitness), which allows reaching the best solution from the point of view of the balance between quality and cost.

2.1. Step i: Electromagnetic mapping of area under study

The first step is to characterize the electromagnetic pollution level of the area object of study. For this purpose, this area is defined as a grid where each cell represents an elemental surface (whose dimensions will be fixed according to the required precision and the total extension of the area of study). Therefore, the area can be mathematically represented by an array where each element contains the average value of the density of magnetic flow at every point.

These (B) values are obtained through different procedures (calcu-

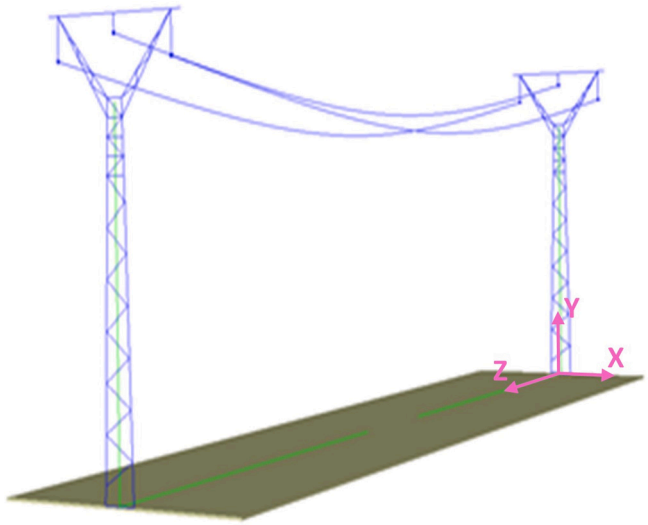

Fig. 2. Reference system location.

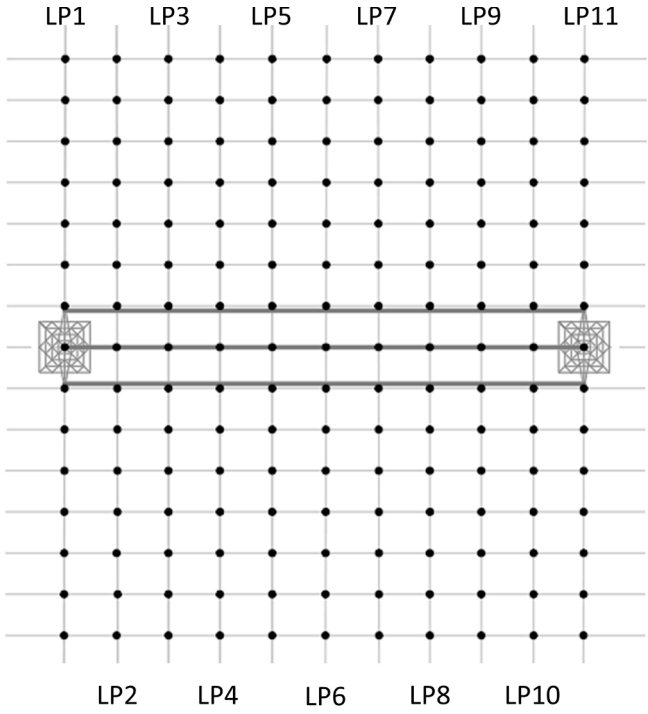

Fig. 3. Longitudinal profile measurement points.

lated, measured or esteemed). It is important to pay attention to, first, the presence of one or multiple sources and, two, the kind of source: power lines or MV/LV substations.

2.1.1. Electromagnetic mapping of power lines environment

Power lines are one of the main sources of electromagnetic pollution in an urban area, both in residential and work environments.

The longitudinal profile of the magnetic field generated by a power line has been defined with 11 lateral profiles. Each side profile contains 15 measurement points.

The decision to take 15 measurements [-30–25 −20–15 −10–5 −2.5 0 2.5 5 10 15 20 25 30 m] to obtain each lateral profile of the magnetic field generated by a power line corresponds to the requirements of Institute of Electrical and Electronics Engineers (2008). This standard states that such a lateral profile shall start at a distance of at least 30 m (100 ft) beyond the outer conductor on one side and progress successively to the same distance from the outer conductor on the opposite side. The standard requires at least five measurements per side, plus the central measurement, making 11 measurements.

It is common not to have all the measurements available for various reasons (private areas, non-accessible areas, roads, etc.) in urban areas. To avoid this inconvenience, the total number of measurements of each lateral profile has been increased to 7 per side (instead of 5), plus the central measurement, making up the 15 measurements used in the chosen protocol.

The 15 values of the magnetic field, $B([x_p], 1, z_s)$, are measured at a height of 1 m $(y = 1)$, perpendicular to the longitudinal axis of the power line and at the distances $[x_p]$, Eq. (1).

$$[x_p] = 5 \bullet [p]; [p] = [-7, \cdots, 0, \cdots, 7] \tag{1}$$

In any case, even if all measurements are available, this increase allows for reducing the error of the estimated values, in accordance with previous results obtained in Muñoz et al. (2013).

For the longitudinal profile, in Institute of Electrical and Electronics Engineers (2008) states that it shall be composed of 11 lateral profiles, which shall (preferably) be located at positions corresponding to 10 consecutive equal (or nearly equal) increments for a total distance equal to one span, Eq. (2).

$$z_s = (s-1) \cdot L/10; \quad s = [[1, 2, \ldots, 11] \tag{2}$$

where L is the span length.

Other authors (Kuusiluoma, Keikko, Hovila, & Korpinen, 2000) also use protocols with an increased number of measurements in the lateral profiles.

Fig. 2 shows the location of the span's axis of the reference system.

Fig. 3 shows the distribution of the 165 (15 × 11) measure points (p) which make up the lateral profiles (LP) of longitudinal profile (s).

For these non-accessible measure points, it is proposed a procedure to reduce the number of necessary measures obtaining the estimated values of these non-accessible points. Fig. 4 represents the flowchart of this procedure.

To each span in each power line, the procedure starts with the location of the points indicated in the measurement protocol (15 × 11).

Starting from Ampere's law, Eq. (3), the application of analytical methods permits obtaining calculated values by means of expressions that, in a general way, present the generated B by power lines as a rational function of the distance to the considered point.

According to principle of superposition, the total B is expressed as the vector sum of the individual supports of the n conductors.

$$[\overline{B}_c([x_p], 1, [z_s])] = \frac{\mu_0}{2\pi} \bullet \sum_{k=1}^{n} \frac{I_{-k} \bullet (\widehat{u}_z \times \overline{R}_k)}{R_k^2} \tag{3}$$

where $[\overline{B}_c]$ is the array of the density of magnetic flow (T) at the points of interest, $\mu_0 = 4\pi \bullet 10^{-7} (V \bullet s/A \bullet m)$ is the magnetic permeability of free space, I_{-k} is the current phasor through the k-th, $\widehat{u}_z$ is the unitary vector in the direction of the line longitudinal axis, $\overline{R}_k$ is the distance vector from the k-th conductor to the field point.

The method applied to obtain these values is proposed in (Filippopoulos & Tsanakas, 2005). The use of double complex numbers allows it to transform Eq. (3) in Eq. (4).

$$\left[B_{-c}([x_p], 1, [z_s])\right] = \frac{j_1 \mu_0}{2\pi} \bullet \sum_{k=1}^{n} \frac{I_{-k}}{\overline{R}_k} \tag{4}$$

where $B_{-}c$ is the magnetic field representation through a double complex number, $\overline{R}_k$ is the position representation through a complex number from the set $(x_k + j_1 y_k)$ and, I_{-k} is the phasor intensity representation through a complex number from the set $I_k \bullet e^{j_2 \varphi_k}$.

Three power line configurations are considered: flat, delta and

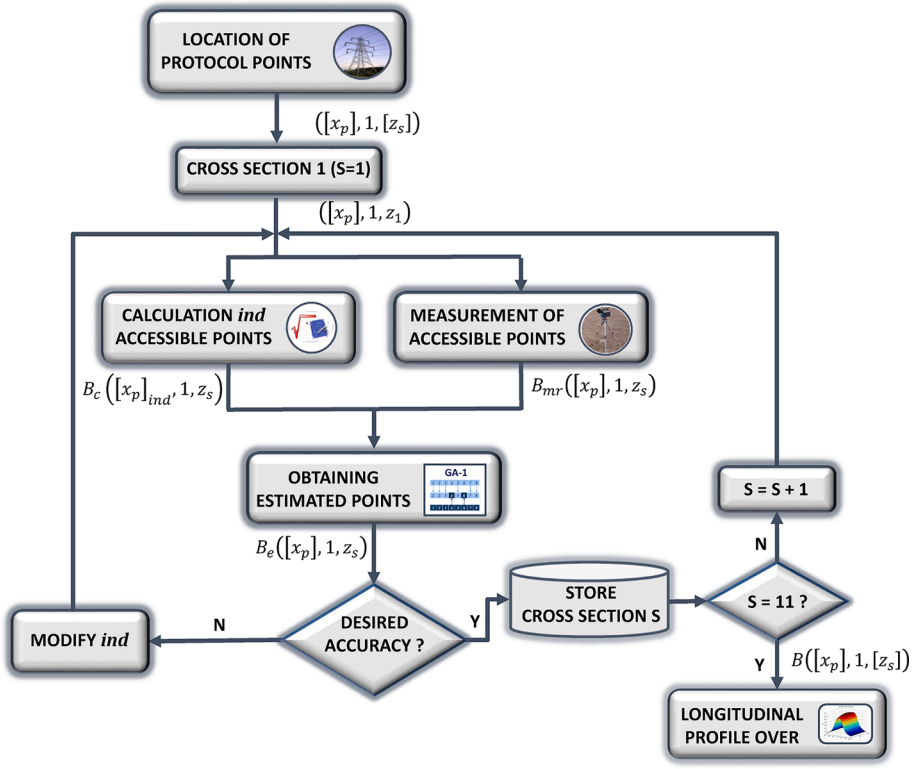

Fig. 4. Operative flowchart.

Table 1
Magnetic field module for the power line configurations used.

Flat	$B_c = \frac{\mu_0 \cdot I \cdot w}{2\pi \cdot R} \sqrt{\frac{3R^2 + w^2}{R^4 - 2R^2 \cdot w^2 \cdot \cos(2\varphi_R) + w^4}}$
Delta	$B_c = \frac{3\sqrt{2} \cdot \mu_0 \cdot I \cdot h}{4\pi} \sqrt{\frac{R^2 + h^2}{R^6 - 2R^3 \cdot h^3 \cdot \cos(3\varphi_{Rp}) + h^6}}$
Double Flag	$B_c = \frac{3I \cdot w \cdot \mu_0}{2\pi} \sqrt{\frac{R^8 + w^2 \cdot R^6 + 2w^4 \cdot R^4 \cdot (\cos(2\varphi_R) - \cos(4\varphi_R)) + w^6 \cdot R^2 + w^8}{R^{12} - 2R^6 \cdot w^6 \cdot \cos(6\varphi_R) + w^{12}}}$

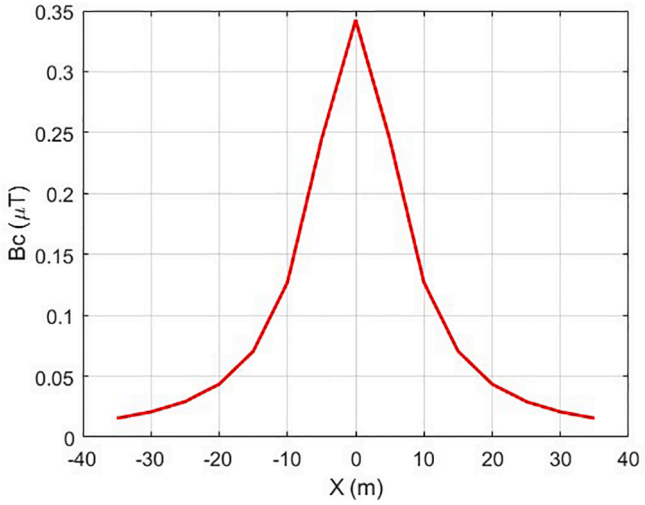

Fig. 5. Calculated values graph.

double flag. Applying simplifications related to the hexagonal symmetry of the chosen configurations. Table 1 shows the equations allow obtaining the magnetic field module (B), reaching a good balance between the quality of the obtained solution and its computational cost. where $\overline{R}$ is the distance vector from the conductors' space distribution center to the field point, h is the distance between a conductor and the centroid, w is the horizontal distance between conductors, and φ_R is the angle between $\overline{R}$, and the horizontal one.

Fig. 5 shows a lateral profile sample, whose values are obtained by the described procedure.

As it can be observed in Fig. 6, in the first step, the B values corresponding to the defined field points in the protocol are divided into two, the disposable or measured values $[B_m([x_p], 1, [z_s])]$, and the non-disposable ones $[B_u([x_p], 1, [z_s])]$.

In a second step, a random subset of measured values $[B_{mt}([x_p], 1, [z_s])]$, is kept as a test set to be later used in the validation (See Table 2).

It is in the third step when the calculated values subset takes part $[B_c([x_p], 1, [z_s])]$, taking over the measured values which are going to be used in the test set $[B_{mt}([x_p], 1, [z_s])]$ and reducing the size of the non-disposable values subset $[B_{ur}([x_p], 1, [z_s])]$. The size adjustment of these subsets is performed iteratively by modifying the percentages of the total measured values (B_m set) used to adjust the variables employing the genetic algorithm (B_{mr} subset) and the one used for the validation of the estimated data (B_{mt} subset). The Euclidean norm is used as the descriptive statistical indicator.

Finally, in the fourth step, the estimated values are obtained $[B_e([x_p], 1, [z_s])]$, following the procedure described in Muñoz et al. (2013). For this, the linear (L_k) and non-linear (NL_k) coefficients are estimated by a GA (GA-1) of Eq. (5):

$$[B_e([x_p], 1, [z_s])] = \sum_{k=1}^{2} L_k \bullet e^{-NL_k \bullet x_p^2} \tag{5}$$

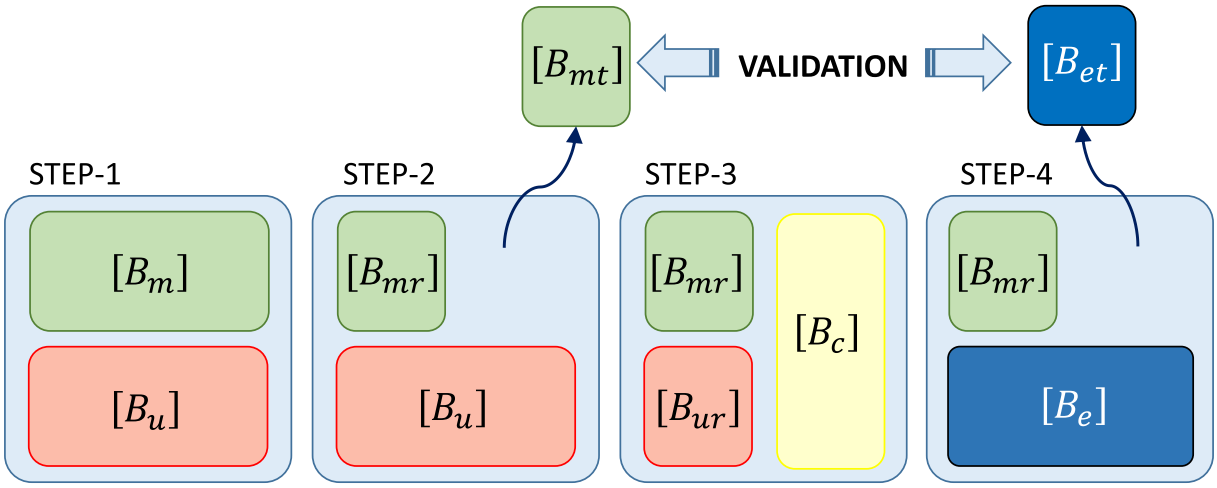

Fig. 6. Distribution of B values subsets.

Table 2
Calculated values.

Xp (m)	−35	−30	−25	−20	−15	−10	−5	0	5	10	15	20	25	30	35
Bc (μT)	0.0155	0.0207	0.0291	0.0435	0.0705	0.1270	0.2444	0.3424	0.2444	0.1270	0.0705	0.0435	0.0291	0.0207	0.0155

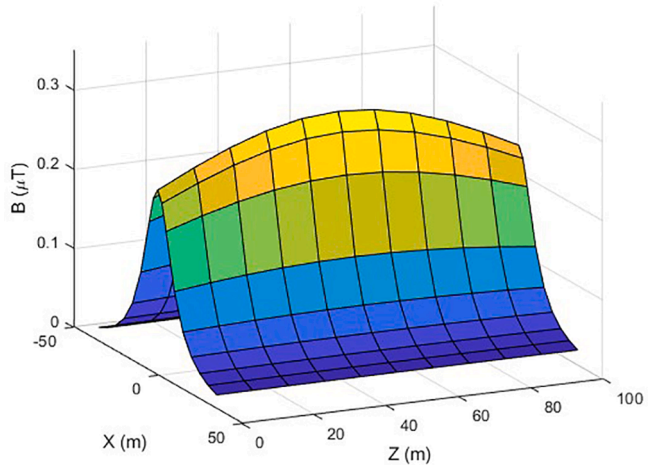

Fig. 7. 3D graph of the longitudinal profile.

Eq. (5) corresponds with the functional approximation used to get the estimated values $[B_e([x_p],1,[z_s])]$ that, together with the non-used values in the test set $[B_{mr}([x_p],1,[z_s])]$, shape each one of the transversal profiles in the span (s).

The validation process is inherent to the GA functioning since it is the final value given by the objective function used. The root medium square error (rmse), Eq. (6), is the one which works as a quality (precision) indicator of the carried out estimation.

$$rmse_s = \sqrt{\frac{\sum\left([B_{mt}([x_p],1,[z_s])] - [B_{et}([x_p],1,[z_s])]\right)^2}{15}} \tag{6}$$

Fig. 7 shows a 3D representation resulting from the discrete integration of the 11 lateral profiles that compose a longitudinal profile obtained by applying the described process.

2.1.2. Electromagnetic mapping of MV/LV substation environment

Other generator sources of magnetic field, usually present in urban environments, are the medium/low voltage substations. The elements that actually function as the main emitting sources in these substations are the voltage busbars.

This work requires a set of measurements taken in the accessible area adjacent to the substation. From these measurements, the parameters that define a magnetic field propagation model based on an attenuation function are obtained. This model allows estimating the B value at any distance.

For a given area, the ratio between the known value of the magnetic field at a point $[B_e([x_g],[z_g])]$ and the unknown value of B at another point $[B_t([x_g],[z_g])]$, depends on a reduction coefficient α, Eq. (7). This reduction coefficient represents the effect of the absorption losses of the transmitting medium (air, buildings, street furniture, etc.) as a function of distance.

$$[B_t(x_g,z_g)] = [B_e([x_g],[z_g])] \bullet e^{-\alpha \bullet r} \tag{7}$$

where r is the side length in each cell of the grid.

The applied procedure, Fig. 8, follows an operative flowchart scheme similar to the one described for power lines.

The set of measured values, $[B_m([x_g],[z_g])]$, are divided into three subsets:

- Measurements at cells annexed to the substation, $[B_{em}([x_g],[z_g])]$.
- Measurements at randomly chosen cells, $[B_{rm}([x_g],[z_g])]$, for the estimation.
- Measurements at randomly chosen cells, $[B_{tm}([x_g],[z_g])]$, to be used as a set test.

The attenuation coefficient value α, is obtained through the application of the subsets $[B_{em}([x_g],[z_g])]$ and $[B_{rm}([x_g],[z_g])]$ to a genetic algorithm (GA-2). This procedure allows minimizing the root mean square error (RMSE), Eq. (8), between the magnetic field values of the test set $[B_{tm}([x_g],[z_g])]$ and the estimated values, $[B_e([x_g],[z_g])]$.

$$RMSE = \sqrt{\frac{\sum\left([B_{mt}([x_g],[z_g])] - [B_e([x_g],[z_g])]\right)^2}{\dim[B_{mt}([x_g],[z_g])]}} \tag{8}$$

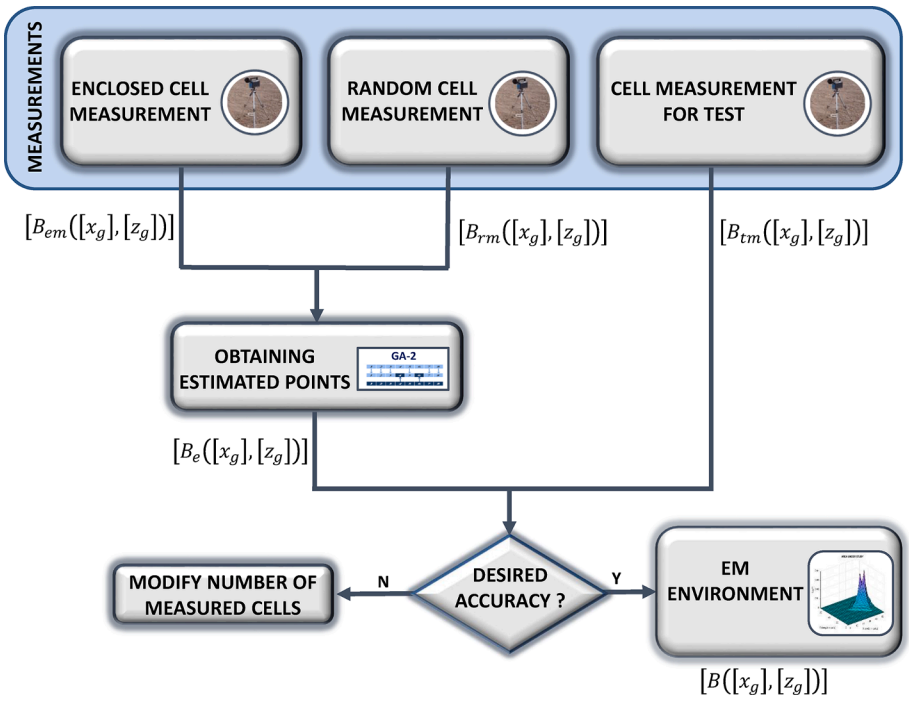

Fig. 8. Operative flowchart.

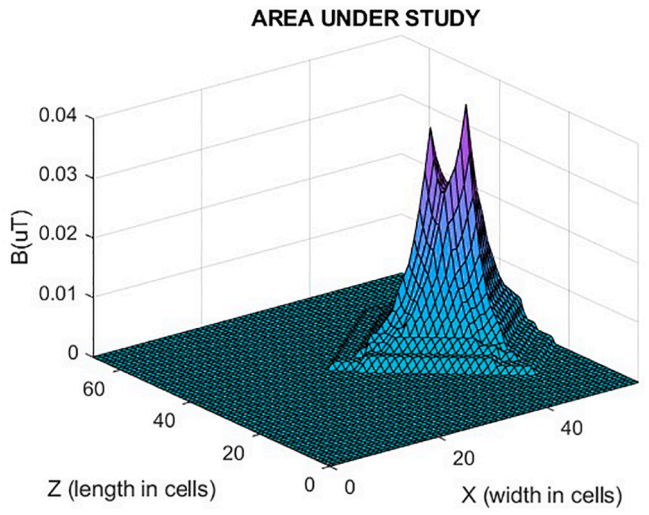

Fig. 9. 3D graph of substation environment.

Fig. 9 shows a 3D chromatic map resulting of the procedure application described in an area with two sources, expressing the values of B in μT.

2.1.3. Multiple sources

The procedures described above make it possible to obtain the magnetic field for the two types of sources studied individually, but considering environments where only one of them is present or, if there are several, one of them is dominant.

Institute of Electrical and Electronics Engineers (2008) states that any source at a distance of 30 m or less influences the magnetic field value. Therefore, the presence of multiple sources is the usual case to consider in urban areas.

When several focuses affect the same field point, it is necessary to know the orientation of the magnetic field vector. The orientation is determined by the application of Ampère's Law (Eq. (3)).

The module and orientation allow the magnetic field vector to be broken down into its three components, the component in the longitudinal direction of the electric line being zero. The sum of the effects is made by adding the magnetic field components of the different focuses affecting the field point and then calculating the module of the resultant.

Finally, it should be noted that having equipment that provides the magnetic field in the three spatial directions makes it possible to validate the module (rms value) and its spatial components.

2.2. Step ii: Trajectories planning of minimal electromagnetic pollution

The minimal electromagnetic pollution trajectory is obtained by GA-3, following the general flowchart shown in Fig. 1.

Anyway, for trajectories planning, a specific procedure to obtain the first generation (initial population) was designed. Fig. 10 shows a flowchart of this process.

First, once the study area has been established in the form of a grid, the waypoints are defined and numbered. These waypoints are the points where the trajectory can change direction. Fig. 11(a) shows a graphical example.

Each directional waypoint is associated to three arrays. Two location arrays (WPx and WPz), Eq. (9) whose elements correspond with the coordinates of each directional waypoint, expressed in cells of the grid.

$$WPx = \begin{pmatrix} WPx_1 & \cdots & WPx_m \\ \vdots & \ddots & \vdots \\ WPx_n & \cdots & WPx_{m\times n} \end{pmatrix} WPz = \begin{pmatrix} WPz_1 & \cdots & WPz_m \\ \vdots & \ddots & \vdots \\ WPz_n & \cdots & WPz_{m\times n} \end{pmatrix} \quad (9)$$

The third array associated is the orientation specific array (WP_O). Eq. (10) shows (WP_O) is a square array of 3x3 dimension. Each element are the number assigned to the potential destination waypoints for each waypoint, according to the chosen orientation. A zero value represents a not achievable direction for a specific waypoint. Fig. 11(b) shows an example of potential directions for the waypoints.

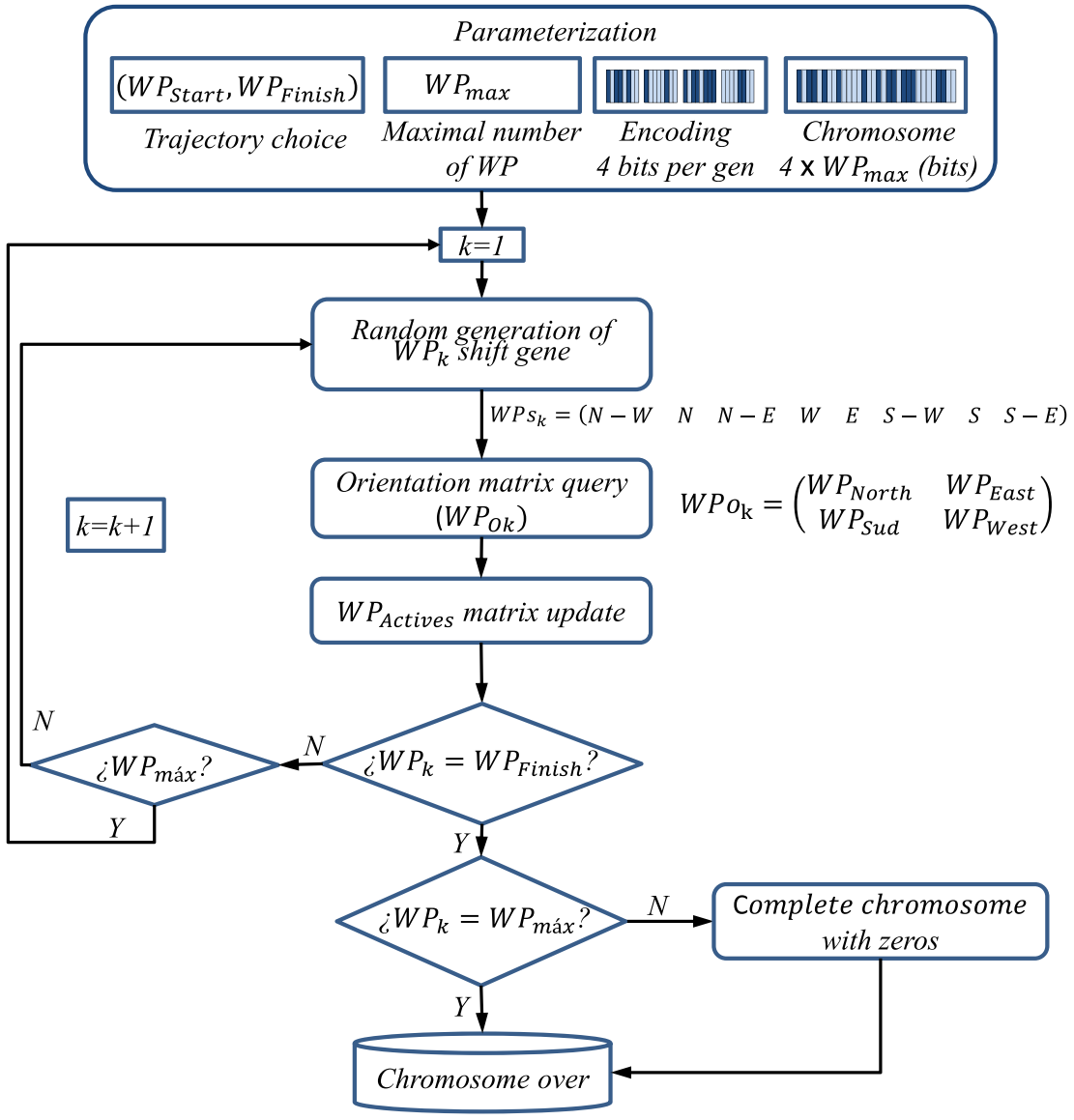

Fig. 10. Flowchart of chromosomes random generation (initial population).

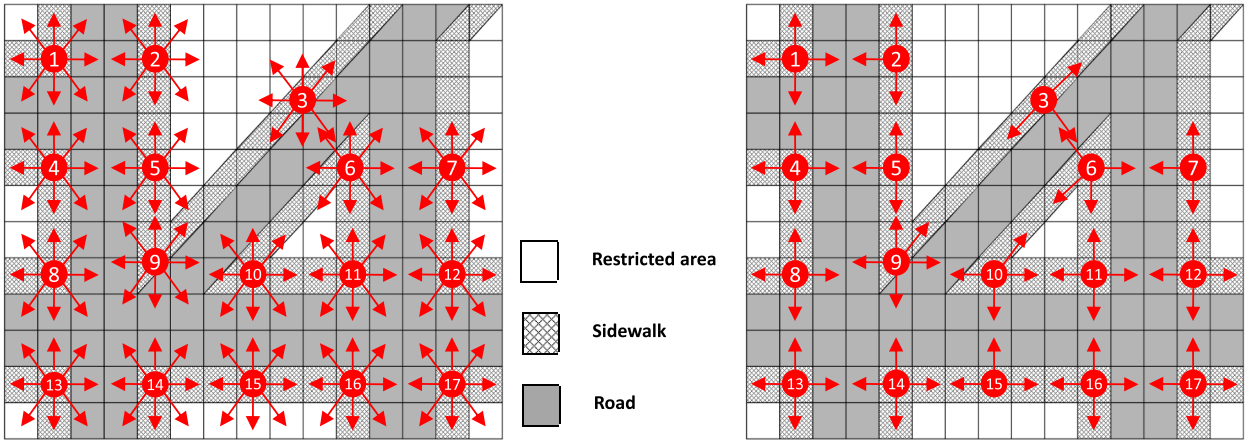

Fig. 11. Grid with directional waypoints.

$$WPo_k = \begin{pmatrix} WP_{North-West} & WP_{North} & WP_{North-East} \\ WP_{West} & WP_K & WP_{East} \\ WP_{South-West} & WP_{South} & WP_{South-East} \end{pmatrix} \rightarrow \begin{cases} \vdots \\ WPo_8 = \begin{pmatrix} 0 & 1 & 0 \\ 1 & 8 & 1 \\ 0 & 1 & 0 \end{pmatrix} \\ WPo_9 = \begin{pmatrix} 0 & 1 & 1 \\ 1 & 9 & 1 \\ 0 & 1 & 0 \end{pmatrix} \\ \vdots \end{cases} \tag{10}$$

Next, the procedure to obtain the solutions (trajectories) that will form the initial population is started. Each of these solutions (trajectories) will be formed by a succession of sectors between the initial waypoint WP_{Start} and the destination waypoint WP_{Finish}. In the example shown in Fig. 11, the WP_{13} and, WP_7, respectively. Each of the stretches that make up a trajectory are identified by the waypoints that define their start and end.

Beginning from WP_{Start} the movement directions for each waypoint are being generated randomly and sequentially (WPs_k). From possible directions offered by a waypoint, the random selection will be made only among those that are included in the quadrant where the line that joins this waypoint (WP_K) with the destination waypoint (WP_{Finish}) is located, Fig. 12(a). In this way, setbacks and intermediate estrangements are avoided, thus ensuring an approach to the final waypoint in each new section that is added to the trajectory.

$$\begin{aligned} &WPs_k = (\ N-W \quad N \quad N-E \quad W \quad E \quad S-W \quad S \quad S-E\ ) \\ &\begin{cases} \vdots \\ WPs_9 = (\ 0 \quad 0 \quad 0 \quad 0 \quad 1 \quad 0 \quad 0 \quad 0\ ) \\ WPs_{10} = (\ 0 \quad 0 \quad 1 \quad 0 \quad 0 \quad 0 \quad 0 \quad 0\ ) \\ \vdots \end{cases} \end{aligned} \tag{11}$$

This generates the array of active waypoints $(WP_{Actives})$. This array has the same dimension of the grid (expressed in cells). All elements are zero, except the cells corresponding to the active waypoints that take value one. Initially, only the cells corresponding to WP_{Start} and WP_{Finish} will take the value 1.

As the movement options are selected according to the orientations taken, the waypoints used (marked with ones) will be activated, as well as all the cells through which the section passes. Fig. 12(b) shows an example of a trajectory.

All cells through which the trajectory passes are marked as active (value 1 is assigned). Eq. (12) shows the composition of the array $(WP_{Actives})$ for an example of trajectory planning.

$$WP_{Actives} = \begin{pmatrix} 0 & 0 & 0 & 0 & 0 & 0 & 0 & 0 & 0 & 0 & 0 & 0 & 0 & 0 & 0 \\ 0 & 0 & 0 & 0 & 0 & 0 & 0 & 0 & 0 & 0 & 0 & 0 & 0 & 0 & 0 \\ 0 & 0 & 0 & 0 & 0 & 0 & 0 & 0 & 0 & 0 & 0 & 0 & 0 & 0 & 0 \\ 0 & 0 & 0 & 0 & 0 & 0 & 0 & 0 & 0 & 0 & 0 & 0 & 0 & 0 & 0 \\ 0 & 0 & 0 & 0 & 0 & 0 & 0 & 0 & 0 & 0 & 1 & 1 & 1 & 1 & 0 \\ 0 & 0 & 0 & 0 & 0 & 0 & 0 & 0 & 0 & 1 & 0 & 0 & 0 & 0 & 0 \\ 0 & 0 & 0 & 0 & 0 & 0 & 0 & 0 & 1 & 0 & 0 & 0 & 0 & 0 & 0 \\ 0 & 0 & 0 & 0 & 0 & 0 & 0 & 1 & 0 & 0 & 0 & 0 & 0 & 0 & 0 \\ 0 & 1 & 1 & 1 & 1 & 1 & 1 & 0 & 0 & 0 & 0 & 0 & 0 & 0 & 0 \\ 0 & 1 & 0 & 0 & 0 & 0 & 0 & 0 & 0 & 0 & 0 & 0 & 0 & 0 & 0 \\ 0 & 1 & 0 & 0 & 0 & 0 & 0 & 0 & 0 & 0 & 0 & 0 & 0 & 0 & 0 \\ 0 & 1 & 0 & 0 & 0 & 0 & 0 & 0 & 0 & 0 & 0 & 0 & 0 & 0 & 0 \\ 0 & 0 & 0 & 0 & 0 & 0 & 0 & 0 & 0 & 0 & 0 & 0 & 0 & 0 & 0 \end{pmatrix} \tag{12}$$

In case of high dimensions, the array $(WP_{Actives})$ may require the application of sparse array representation techniques or specific techniques, such as the one used in Ji, Guo, Gao, Gong, and Wang (2021).

Setting a maximum number of active waypoints allows working with chromosomes of constant length (the number of stretches may vary). The generated solutions containing the maximum number of active waypoints that do not reach the WP_{Finish} will be rejected.

The choice of a maximum number of active waypoints also allows modifying the balance between exposure and distance. The lower the number of active waypoints, the more valid solutions generated will prioritize the lower exposure (lower number of B values involved in the fitness function setting) over distance.

Each generated solution (chromosome) forms the initial population and the binary coding will have as many genes as the number of maximum sectors selected. Each gene will be consist of the displacement vector containing the orientation of the change of direction at that waypoint (Table 3).

The generated solution (chromosome) is formed by binary codification of the chosen orientations to each active waypoint (genes).

The quality evaluation of each generated trajectory is obtained by adding the elements of the product array (term to term) between the B array and the active waypoint's array (WP_a), Eq. (13).

$$Fitness = \sum \begin{pmatrix} B_{11} \bullet WP_{Actives_{11}} & \cdots & B_{1m} \bullet WP_{Actives_{1m}} \\ \vdots & \ddots & \vdots \\ B_{n1} \bullet WP_{Actives_{n1}} & \cdots & B_{nm} \bullet WP_{Actives_{nm}} \end{pmatrix} \tag{13}$$

Following the flow chart presented in Fig. 1, the selection, crossover, and mutation operators are then applied to evolve the GA.

The selection operator corresponds to a simple reduction procedure, where the generational renewal rate is constant.

The crossover operator is applied to a trajectory (parent solution) where one allele is randomly selected as a crossover point (WP_{KX}) from which two new descendants are generated:

The first descendant consists of the sectors contained between the start waypoint (WP_{Start}) and the crossover waypoint (WP_{KX}). The remaining sectors up to the WP_{Finish} are chosen randomly. The applied generation format favors the work in intensity of the GA.

The second descendant requires randomly selecting a partial trajectory between the initial waypoint (WP_{Start}) and the crossing waypoint (WP_{KX}). The complete trajectory is formed by adding to the partial trajectory obtained the sectors of the parent chromosome between the crossover waypoint (WP_{KX}) and the final waypoint (WP_{Finish}). The generation format applied favors the work in extension of the GA.

For long distances, whose trajectories include a high number of waypoints, the applied operator can contain several crossover points (n), where n + 1 is new descendant generated by each parent.

The mutation operator is applied during the creation of a descendant, releasing the imposed constraint that requires the selection of an direction contained in the quadrant in which the connecting line to the target waypoint is located (WP_{Finish}).

Finally, a high value is set for the convergence criterion (>95%) to compensate for the randomness of the initial parameterization and the variability of the different operators of the genetic algorithm.

The convergence time is not a critical parameter in the proposed application. In any case, there are alternative criteria to reduce the convergence time, such as the one used in Guo, Zhang, Gong, Zhang, and Yang (2019).

3. A case study

The application of the proposed procedure is carried out in the following stages:

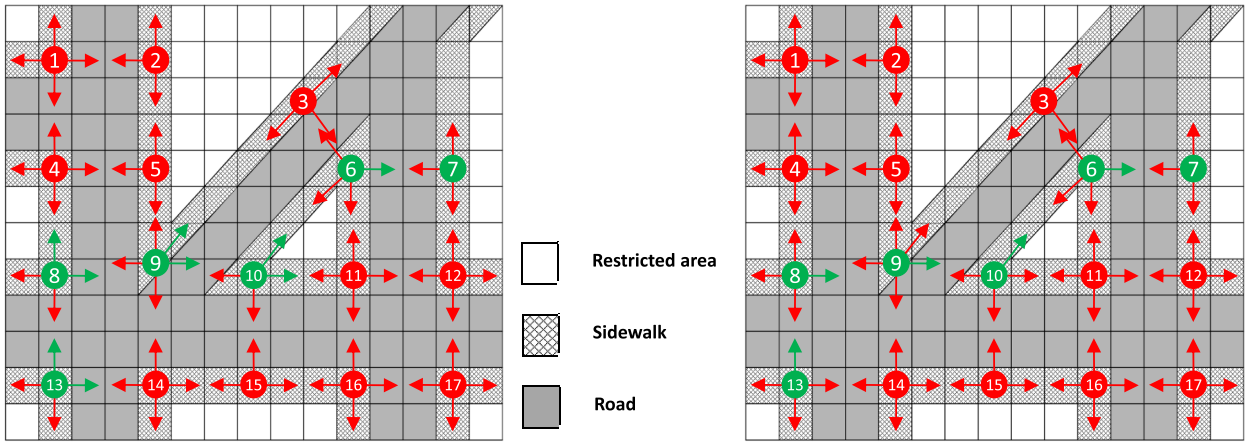

Fig. 12. Trajectory planning.

Table 3
Stretches of the generated trajectory.

Stretches	WP_a	Stretches Def.	Orientation	Shift Vector
1	$WP_{Start} = WP_{13} \rightarrow WP_8$	$WP_{13} \rightarrow WP_8$	North	(0 1 0 0 0 0 0 0)
2	$WP_8 \rightarrow WP_9 \rightarrow WP_{10}$	$WP_8 \rightarrow WP_{10}$	East	(0 0 0 0 1 0 0 0)
3	$WP_{10} \rightarrow WP_6$	$WP_{10} \rightarrow WP_6$	North-East	(0 0 1 0 0 0 0 0)
4	$WP_6 \rightarrow WP_7 = WP_{Finish}$	$WP_6 \rightarrow WP_7$	East	(0 0 0 0 1 0 0 0)

a) Choice of the object of study area.

The studied area was selected by applying three criteria:

- Presence of polluting sources of different nature and features, with the possibility of disposing of both geometrical and electrical data.
- High traffic level, as well as in people and in vehicles.
- Zones of both easy access and orography which allows the location in the accessible areas of the largest numbers of the indicated points by the chosen protocol and to carry out the taking of measures in B.

The chosen zone (Fig. 13) takes up an urban area of 330,000 m^2 (550 × 600 m), located in the city of Malaga (Spain).

b) Establishment of the initial and destination waypoints, as well as the optional waypoint maximum number, which will shape each trajectory.

c) Identification and parameterization of the polluting sources.

Fig. 13 presents the location of the different polluting sources present in the selected area under studio, whose general data are shown in Table 4.

d) Design of the magnetic field grid.

Upon the area object of study, the application of a grid formed by cells which represent elemental surfaces of 5x5 square meters is chosen.

Next, the constraints of our search space are applied, limiting it to those cells which take up accessible and passable surfaces, which coincide with streets and public spaces.

In the case of a pedestrian route, the corresponding constraints to pavements and public road crossings will be added, in the case of a vehicle route, the corresponding ones to the traffic orders, and finally, in the case of bicycles, the one of the bike lane stretch.

e) Obtaining the B values in the grid.

The 13,200 B values of the cells set which make up the cells dimension array 110 × 120, which represents the area grid under study, are obtained starting from the theoretical (calculated), empirical (measured) and valued (algorithmic) procedures, defined in Sections 2.1 and 2.2.

f) Parameterization and application of GA-1 and GA-2.

Table 5 shows the used values in the parameterization of the GAs used to get the B values of each cell in the grid, beginning with the contributions of the power lines sources (GA-1) and the sources corresponding to MV/LV substations (GA-2).

The GAs parameterization which appears in Table 5, has been carried out beginning with accomplished tests following the suitable recommendations in Alander (1992) and Baker (1985).

Table 6 shows the values of the linear and non-linear coefficients, Eq. (5), obtained with GA-2 for the sources.

GA-1 allows obtaining the final values of the attenuation coefficients, Eq. (7), for sources TS-1, TS-2, TS-3 and TS-4 (Table 7).

Fig. 14 shows a 3D chromatic map of B values a 3D.

g) Trajectories' planning.

The trajectories' planning is initiated with the establishment of space constraints and valid solutions.

In a general way, constraints are brought up as zeros into orientation arrays of directional waypoints (WPo_k).

On the other hand, those cells which are corresponded with "restricted areas", are marked in white in the chromatic map (Fig. 15) and they represent private areas, buildings, etc, and they are penalized assigning them higher B values. This same value is used as a constraint, so that it will be eventually considered that a trajectory acquires the

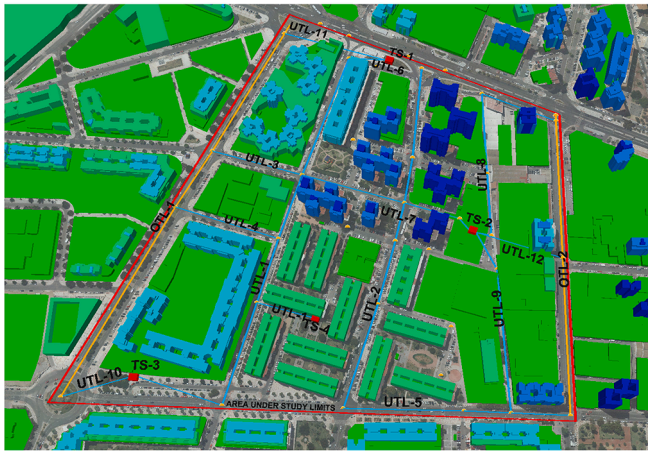

Fig. 13. Location of EMP emission sources.

Table 4
General data on polluting sources.

Acronym	Type	Parameters
TS-1	MV/LV Substation	20/0.4 kV − 1x1 MVA
TS-2	MV/LV Substation	20/0.4 kV − 2x1 MVA
TS-3	MV/LV Substation	20/0.4 kV − 1x1 MVA
TS-4	MV/LV Substation	20/0.4 kV − 1x0.55 MVA
OTL-1	Overhead Transmission Line	20 kV - Flat
OTL-2	Overhead Transmission Line	20 kV - Delta
UTL-1	Underground Transmission Line	20 kV
UTL-2	Underground Transmission Line	20 kV
UTL-3	Underground Transmission Line	20 kV
UTL-4	Underground Transmission Line	20 kV
UTL-5	Underground Transmission Line	20 kV
UTL-6	Underground Transmission Line	20 kV
UTL-7	Underground Transmission Line	20 kV
UTL-8	Underground Transmission Line	20 kV
UTL-9	Underground Transmission Line	20 kV
UTL-10	Underground Transmission Line	20 kV
UTL-11	Underground Transmission Line	20 kV
UTL-12	Underground Transmission Line	20 kV

Table 5
Adjustment values of GA-1 & GA-2.

Parameters	GA-1 Value	GA-2 Value
Generations/ Population	25/100	65/30
Probability of cross	0.80	0.80
Probability of mutation	0.02	0.06
Codification	Binary	
Length of gene	16 bits	
Length of chromosome	4 × 16 = 64 bits	16 bits
Selection operator	Deterministic tournament (p = 2)	Simple reduction(average value)
Crossover operator	Single point	
Fitness function	rmse	
Stop condition	Accuracy achieve	

condition of a possible solution when it obtains a lesser fitness than such a value, thus assuring that every and each one of the stretches in which the solution trajectory consist go through accessible and transitory areas. In the case of motor vehicles trajectories or bicycles, the restricted areas will also include the conditions laid by the traffic regulations and the bike lane stretch.

Table 6
Linear and non-linear coefficients values.

Source	L_{k1}	L_{k2}	NL_{k1}	NL_{k2}
OTL-1	0.0357016	0.81650100	0.08820750	0.00268978
OTL-2	0.0283990	0.380956505	0.08820750	0.00268978
UTL-1	0.0470612	0.631299350	0.08820750	0.00268978
UTL-2	0.0470612	0.631299350	0.08820750	0.00268978
UTL-3	0.0324560	0.435378862	0.08820750	0.00268978
UTL-4	0.0259648	0.348303090	0.08820750	0.00268978
UTL-5	0.0324560	0.435378862	0.08820750	0.00268978
UTL-6	0.0227192	0.304765204	0.08820750	0.00268978
UTL-7	0.0227192	0.304765204	0.08820750	0.00268978
UTL-8	0.0324560	0.435378862	0.08820750	0.00268978
UTL-9	0.0324560	0.435378862	0.08820750	0.00268978
UTL-10	0.0227192	0.304765204	0.08820750	0.00268978
UTL-11	0.0259648	0.348303090	0.08820750	0.00268978
UTL-12	0.0259648	0.348303090	0.08820750	0.00268978

Table 7
Attenuation coefficient values.

Source	α
TS-1	0.02110
TS-2	0.04460
TS-3	0.02110
TS-4	0.01022

To finish with this stage, it will be needed to obtain the border magnetic field values in the area under study, since there may be external sources whose effects could affect the associated field values with the cells of our grid.

h) Application of the GA-3.

The application of the genetic algorithm (GA-3) makes it possible to obtain the waypoints that delimit the different stretches which along with the start and end of the movement, define the optimized trajectory of minimum electromagnetic pollution.

Table 8 shows the adjustment values of the rest of the GA-3 parameters.

As it can be observed in Table 8, the number of generations and solutions which makes up the population, varies, depending on the number of maximum waypoints selected for the trajectory.

Fig. 16 shows an example of the result generated by the proposed procedure for a walk, Fig. 16(a), car, (b) or bicycle trip, (c) between two points in the area under study.

In the first trajectory (yellow), corresponding to the walking route, the stretch is estimated without any kind of additional constraints to the ones already commented upon the limitations to accessible and passable areas. In the second (red) and the third (white) trajectories, the searching space is limited by the traffic constraints corresponding to the traffic regulations and the roads which have bicycle lane.

i) Integration of the results into a Geographic Information System.

Finally, and as it is shown in Fig. 17, the obtained trajectories for the different options (pedestrian, motor vehicle, bicycle) are integrated in a geographic information system (ArcMap (Release 10.6.1), 2018).

4. Discussion

The proposal aims, first, to achieve a decrease in the number of measurements required to obtain the complete mapping and, second, with the same number of available measurements, to obtain a higher quality mapping (lower error) at the points where the magnetic field value has been estimated, compared to the methods proposed by other

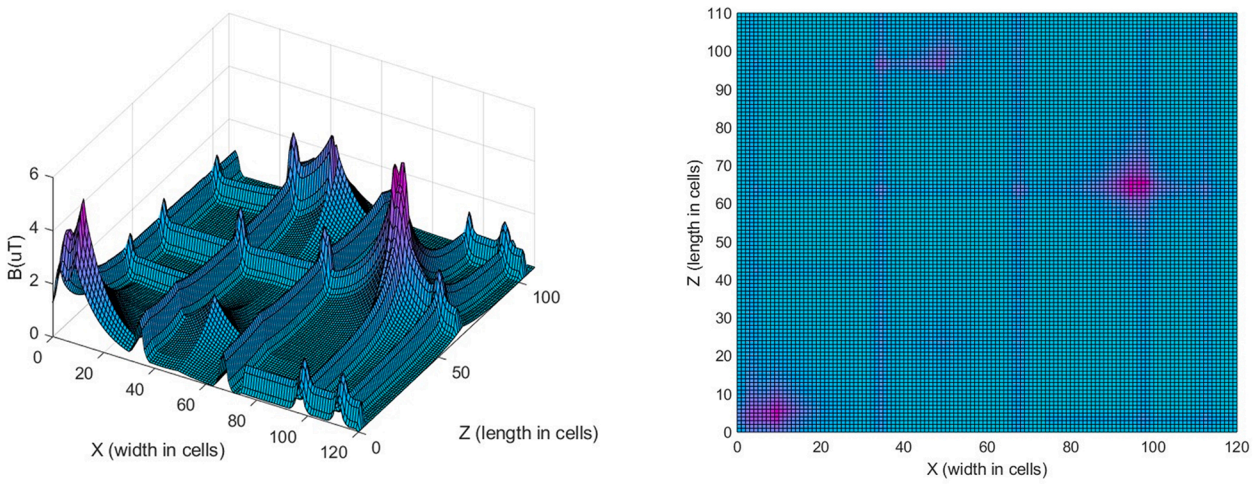

Fig. 14. Area under study 3D-ELP mapping (full view).

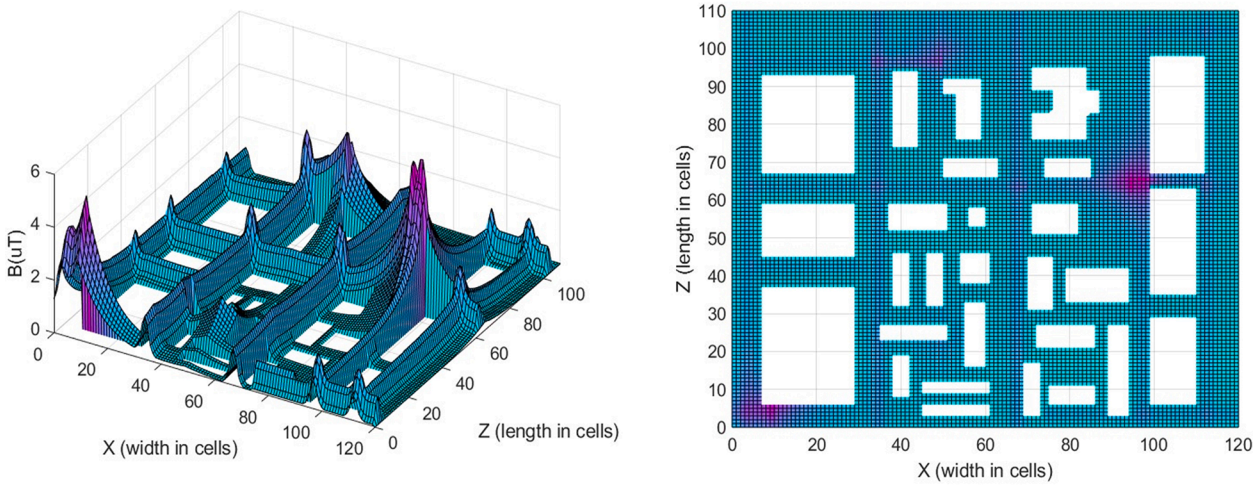

Fig. 15. Area under study 3D-ELP mapping (with restricted areas).

Table 8
Adjustment values of GA-3 parameters.

Parameters	GA-3 Value
Generations/Population	(25 to 85)/(50 to 320)
Probability of cross	0.80
Probability of mutation	0.08
Codification	Binary
Length of gene	2 bits
Length of chromosome	$2{\cdot}WP_{max}$
Selection operator	Simple reduction (constant value)
Crossover operator	Single point
Fitness function	Add

authors, (de Andrade et al., 2020; Fontgalland & de Andrade, 2021; Kurnaz & Mutlu, 2020).

The techniques compared include deterministic methods such as Cubic Spline and Inverse Distance Weighting (IDW and IDW2) and stochastics such as Ordinary Kriging.

To evaluate the quality of the results among these techniques and the proposed approach, five usual measures of error of fit are used: mean absolute error (MAE), Eq.(14), mean absolute percentage error (MAPE), Eq. (15), mean square error (MSE), Eq. (16), root mean square error (RMSE), Eq. (17), and normalized root mean square error (NRMSE), Eq. (18).

$$MAE = \frac{1}{n} \bullet \sum_{i=1}^{n} |B(x) - \widehat{B}(x)| \tag{14}$$

$$MAPE = \frac{1}{n} \bullet \sum_{i=1}^{n} \frac{|B(x) - \widehat{B}(x)|}{B(x)} \bullet 100 \tag{15}$$

$$MSE = \frac{1}{n} \bullet \sum_{i=1}^{n} (B(x) - \widehat{B}(x))^2 \tag{16}$$

$$RMSE = \sqrt{\frac{1}{n} \bullet \sum_{i=1}^{n} (B(x) - \widehat{B}(x))^2} \tag{17}$$

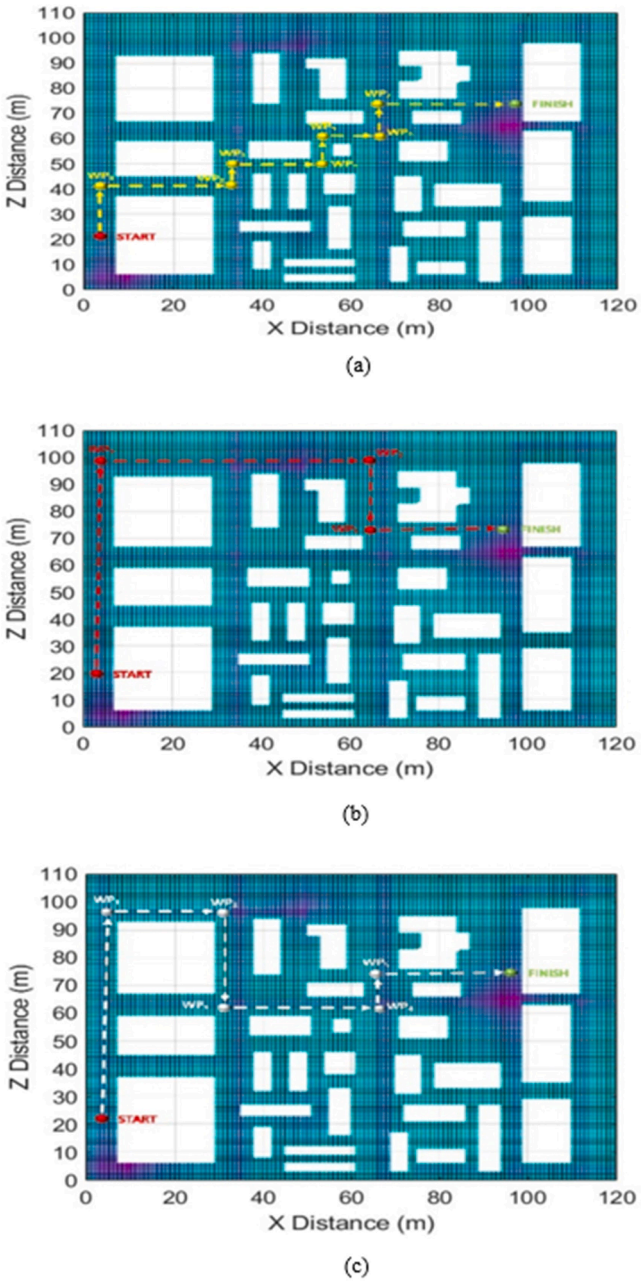

Fig. 16. GA-3 Generated trajectories.

$$NRMSE = \frac{\sqrt{\frac{1}{n} \bullet \sum_{i=1}^{n} (B(x) - \widehat{B}(x))^2}}{max(B) - min(B)} \tag{18}$$

Figs. 18 and 19 plot the results obtained in the UTL-2 and TS-1 with three intermediate control points.

Figs. 18 and 19 show graphically that the proposed GA-based method achieves a better fit with the measured values than the other methods, for both power lines and substations.

Table 9 shows the results of the fit error obtained in the MV/LV substation environment, and Table 10 shows those obtained for the power line environment. It is verified that the proposed GA-based method obtains a magnetic field estimation with lower error than the other methods.

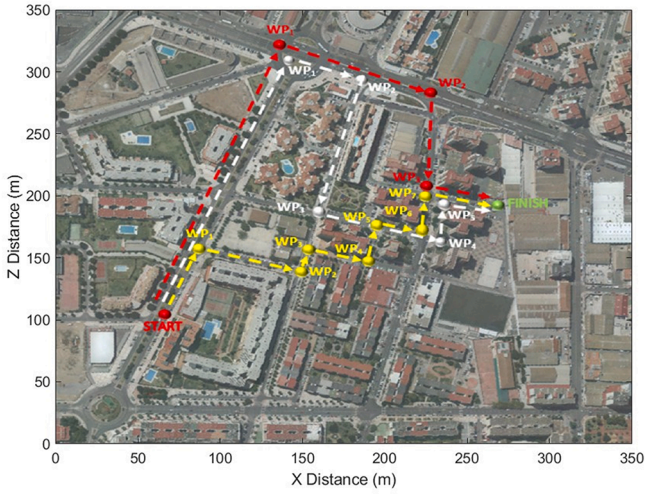

Fig. 17. Integration of trajectories into a geographic information system.

All the indicators used show that the proposed GA-based method obtains a magnetic field estimation with lower error than the rest of the methods.

5. Conclusions

This paper presents a comprehensive approach for, first, mapping electromagnetic pollution of complete urban areas and, second, based on the former data, trajectories planning of commuting with minimal electromagnetic exposure.

In the first stage, an analytical approach is proposed to reduce the number of measurements, supplementing them with theoretical (calculated) and estimated (algorithmic) ones. For the estimated values, using GA allows obtaining these values with lower error than those proposed by previous works, based on interpolation techniques. Furthermore, this proposal considers the superposition effect of electromagnetic field generated by multiple sources at industrial frequency, considering two different kinds in urban areas: power lines (overhead or underground) and medium/low voltage substations.

This reduction in required measurements supposes the saving in equipment, human resources and time. Furthermore, it accurately solves the problem that measuring at specific points in urban areas is not always possible. The proposed approach achieves a complete electromagnetic pollution mapping with lower error than the interpolation methods proposed in previous works, 1% in power lines and 2.5% in medium/low voltage substations.

For the first time, a method for trajectories planning of commuting with minimal electromagnetic exposure is proposed in the second stage. For this, an ad hoc defined searching space allows the use of GA to obtain an optimized trajectory. In this optimization, both distance and pollution exposure are considered. These two parameters are configurable by the user (pedestrian, biker o driver) being able to choose between the limits of a lower electromagnetic exposure and a longer distance or vice versa, enabling a configurable balanced solution between both extremes.

It should be noted that the results obtained could be integrated into geographic information systems in both portable geolocation devices (GPS) and mobile applications.

The limitations of the proposed approach are related to the number of elements considered. On the mapping stage, the number of magnetic sources considered, and on the second stage, the number of waypoints of

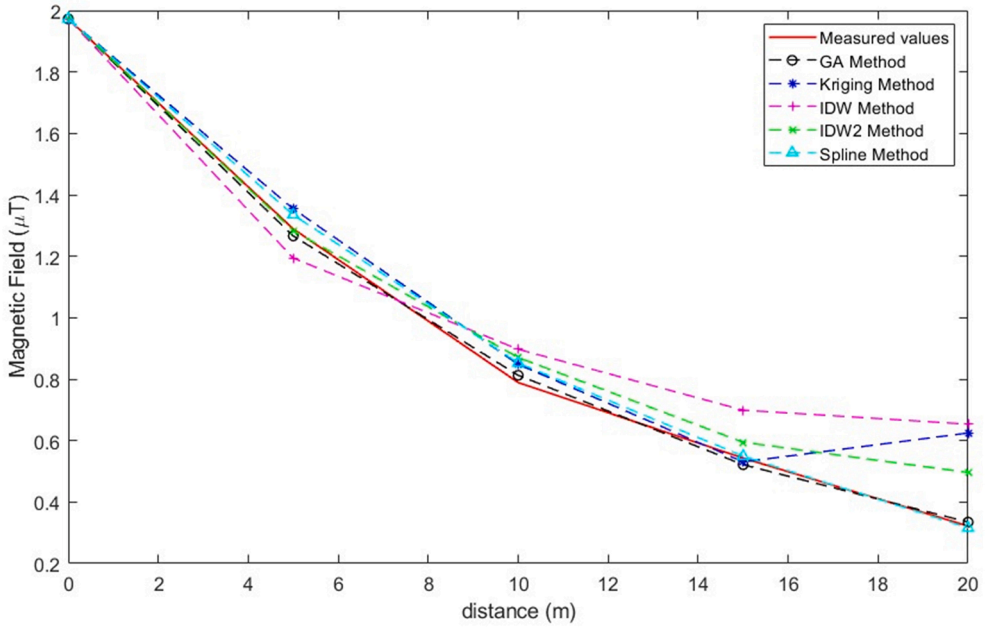

Fig. 18. MV/LV substation environment.

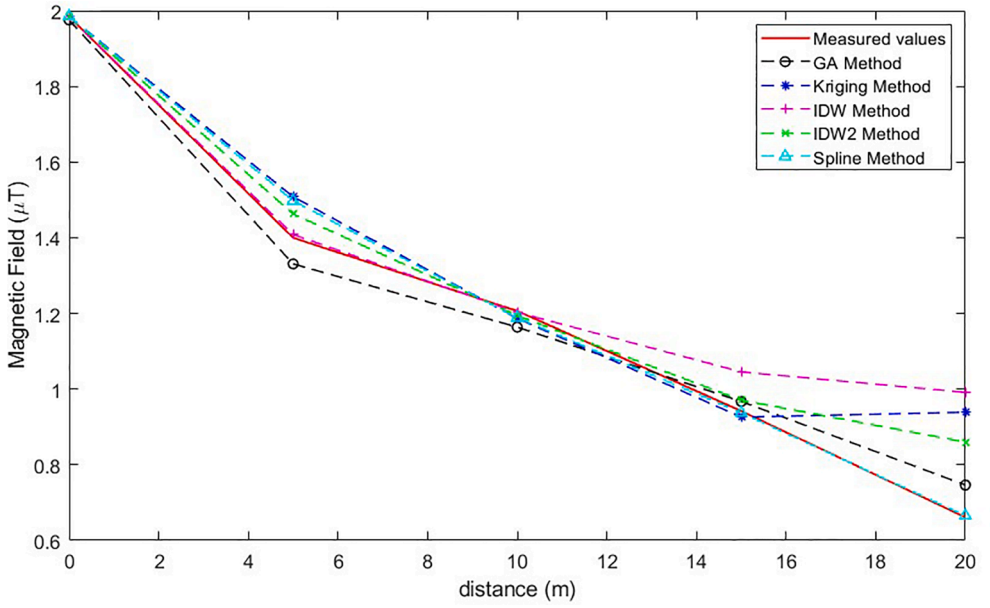

Fig. 19. Power line environment.

Table 9
MV/LV substation environment. Measures of fit.

	Genetic lgorithm	Ordinary Kriging	IDW	IDW2	Cubic Spline
MAE (μT)	**0.0160**	0.0989	0.1383	0.0625	0.0244
MAPE (%)	**2.2919**	25.4213	30.6074	14.8716	2.9393
MSE (μT^2)	**0.0004**	0.0278	0.0311	0.0079	0.0012
RMSE (μT)	**0.0201**	0.1666	0.1764	0.0891	0.0353
NRMSE	**0.0122**	0.1010	0.1069	0.0540	0.0214

Table 10
Power line environment. Measures of fit.

	Genetic Algorithm	Ordinary Kriging	IDW	IDW2	Cubic Spline
MAE (μT)	**0.0108**	0.0840	0.0739	0.0516	0.0760
MAPE (%)	**0.8859**	8.2114	7.9117	4.7559	7.3621
MSE (μT^2)	**0.0002**	0.0124	0.0102	0.0052	0.0103
RMSE (μT)	**0.0128**	0.1113	0.1008	0.0722	0.1014
NRMSE	**0.0106**	0.0922	0.0835	0.0598	0.0840

the studied area. The increase in these numbers implies an increase in the computational cost and, therefore, in the resources required.

Future investigations should be oriented in three directions: i) the use of adaptive GA to maintain up-to-date electromagnetic pollution maps of entire urban areas, ii) include exposure time among the configurable options for optimal trajectory determination, and iii) penalize trajectories with critical exposure stretches.

Declaration of Competing Interest

The authors declare that they have no known competing financial interests or personal relationships that could have appeared to influence the work reported in this paper.

Data availability

Data will be made available on request.

Acknowledgment

Financing for open access position: University of Malaga / CBUA.

References

Alander, J. (1992). On optimal population size of genetic algorithms. In *Proceedings Computer Systems and Software Engineering (CompEuro)* (pp. 65–70). https://doi.org/10.1109/CMPEUR.1992.218485

Alijuan, L., Wanzhong, Z., Xuyun, Q., Xibo, W., Xin, H., & Baoyi, W. (2018). Intelligent electric vehicle trajectory optimization method based on improved genetic algorithm. *Joint International Conference on Energy, Ecology and Environment (ICEEE 2018) and International Conference on Electric and Intelligent Vehicles (ICEIV 2018)*. https://doi.org/10.12783/DTEEES/ICEEE2018/27778.

ArcMap (Release 10.6.1). (2018). Windows. Environmental Systems Research Institute.

Asadi, D., & Atkins, E. (2018). Multi-objective weight optimization for trajectory planning of an airplane with structural damage. *Journal of Intelligent & Robotic Systems, 91*, 667–690. https://doi.org/10.1007/s10846-017-0753-9

Baker, J. (1985). Adaptive selection methods for genetic algorithms. In *Proceedings of the International Conference on Genetic Algorithms and Their Applications*. https://doi.org/10.4324/9781315799674

Chai, R., Savvaris, A., Tsourdos, A., Chai, S., & Xia, Y. (2019). Stochastic spacecraft trajectory optimization with the consideration of chance constraints. *IEEE Transactions on Control Systems Technology, 28*(4), 1550–1559. https://doi.org/10.1109/TCST.2019.2908938

Cruz, P., Hoeffelman, J., & del Pino, J. (2008). Passive loop-based mitigation of magnetic fields from underground power cable. *IEEE Latin America Transactions, 6*(1), 59–65. https://doi.org/10.1109/TLA.2008.4461633

de Andrade, H., Figueiredo, A., Fialho, B., Paiva, J., Queiroz, I., & Sousa, M. (2020). Analysis and development of an electromagnetic exposure map based in spatial interpolation. *Electronics Letters, 56*(8), 373–375. https://doi.org/10.3390/en12071332

del-Pino-López, J., Cruz-Romero, P., Serrano-Iribarnegaray, L., & Martínez-Román, J. (2014). Magnetic field shielding optimization in underground power cable duct bank. *Electric Power Systems Research, 114*, 21–27. https://doi.org/10.1016/j.epsr.2014.04.001

del-Pino-López, J., Giaccone, L., Canova, A., & Cruz-Romero, P. (2015). Design of active loops for magnetic field mitigation in MV/LV substation surroundings. *Electric Power System Reserch, 119*, 337–344. https://doi.org/10.1016/j.epsr.2014.10.019

Filchev, L., Teodosiev, D., Nedkov, R., Borisova, D., Kehayov, B., Iliev, I., & Tsvetkov, T. (2019). Web-based EMF monitoring in urban environment. *Seventh International Conference on Remote Sensing and Geoinformation of the Environment (RSCy2019) (pp. 1117415)*. https://doi.org/10.1117/12.2533559.

Filippopoulos, G., & Tsanakas, D. (2005). Analytical calculation of the magnetic field produced by electric power line. *IEEE Transactions on Power Delivery, 20*(2), 1470–1482. https://doi.org/10.1109/TPWRD.2004.839184

Fogel, L., Owens, A., & Walsh, M. (1966). *Artificial intelligence through simulated evolution*. New York, NY: John Wiley & Sons Inc.

Fontgalland, G., & de Andrade, H. (2021). Estimation of electric and magnetic fields in a 230 kV electrical substation using spatial interpolation techniques. *IET Science, Measurements & Technology, 15*(4), 411–418. https://doi.org/10.1049/smt2.12038

Goldberg, D. (1989). *Genetic algorithms in search, optimization and machine learning*. Boston, MA: Addison-Wesley Longman Publishing.

Guo, F., Luo, W., Gui, F., Zhu, J., You, Y., & Xing, F. (2020). Efficiency analysis and Integrated design of rocket-augmented turbine-based combined cycle engines with trajectory optimization. *Energies, 13*(11), 2911. https://doi.org/10.3390/en13112911

Guo, Y., Yang, H., Chen, M., Cheng, J., & Gong, D. (2019). Ensemble prediction-based dynamic robust multi-objective optimization methods. *Swarm and Evolutionary Computation, 48*, 156–171. https://doi.org/10.1016/j.swevo.2019.03.015

Guo, Y., Zhang, X., Gong, D., Zhang, Z., & Yang, J. (2019). Novel interactive preference-based multiobjective evolutionary optimization for bolt supporting networks. *IEEE Transactions on Evolutionary Computation, 24*(4), 750–764. https://doi.org/10.1109/TEVC.2019.2951217

Institute of Electrical and Electronics Engineers, (2008). *IEEE standard procedures for measurement of power frequency electric and magnetic fields from AC power lines (Std. 644)*. https://doi.org/10.1109/IEEESTD.1995.122621.

International Commission on Non-Ionizing Radiation Protection. (2010). Guidelines for limiting exposure to time-varying electric and magnetic fields (1 Hz to 100 kHz). *Health Physics, 99*(6), 818–836. https://doi.org/10.1097/HP.0b013e3181f06c86

Ji, J., Guo, Y., Gao, X., Gong, D., & Wang, Y. (2021). Q-learning-based hyperheuristic evolutionary algorithm for dynamic task allocation of crowdsensing. *IEEE Transactions on Cybernetics, 1–14*. https://doi.org/10.1109/TCYB.2021.3112675

Kuo, Y., Lin, C., & Lin, Z. (2020). Dual-optimization trajectory planning based on parametric curves for a robot manipulator. *International Journal of Advanced Robotic Systems, 17*(3), 1729881420920046. https://doi.org/10.1177/1729881420920046.

Kurnaz, C., & Mutlu, M. (2020). Comprehensive radiofrequency electromagnetic field measurements and assessments: A city center example. *Environmental Monitoring and Assessment Research, 192*(6), 1–14. https://doi.org/10.1007/s10661-020-08312-3

Kuusiluoma, S., Keikko, T., Hovila, J., & Korpinen, L. (2000). Comparison of electric and magnetic fields from electric power systems with exposure recommendations of the European Union. *PowerCon 2000. International Conference on Power System Technology. Proceedings (Cat. No. 00EX409), 2*, (pp. 843-848). https://doi.org/10.1109/ICPST.2000.897131.

Lee, G., Mallipeddi, R., & Lee, M. (2017). Trajectory-based vehicle tracking at low frame rates. *Expert Systems with Applications, 80*, 46–57. https://doi.org/10.1016/j.eswa.2017.03.023

Liu, J., Wei, M., Li, H., Wang, X., Wang, X., & Shi, S. (2020). Measurement and mapping of the electromagnetic radiation in the urban environment. *Electromagnetic Biology and Medicine, 39*(1), 38–43. https://doi.org/10.1080/15368378.2019.1685540

Long, Z., Jiang, Z., Wang, C., Jin, Y., Cao, Z., & Li, Y. (2020). A novel approach to control of piezo-transducer in microelectronics packaging: PSO-PID and editing trajectory optimization. *IEEE Transactions on Components, Packaging and Manufacturing Technology, 10*(5), 795–805. https://doi.org/10.1109/TCPMT.2020.2984701

Lucca, G. (2016). Electromagnetic interference at power frequencies: Shielding factor related to an urban environment. *IET Science, Measurement & Technology, 10*(6), 614–620. https://doi.org/10.1049/iet-smt.2016.0016

Madridano, Á., Al-Kaff, A., Martín, D., & de la Escalera, A. (2021). Trajectory planning for multi-robot systems: Methods and applications. *Expert Systems with Applications, 173*, Article 114660. https://doi.org/10.1016/j.eswa.2021.114660

Melnick, R. (2020). Regarding ICNIRP's evaluation of the national toxicology program's carcinogenicity studies on radiofrequency electromagnetic fields. *Health Physics, 118*(6), 678–682. https://doi.org/10.1097/HP.0000000000001268

Muñoz, F., Aguado, J., Martín, F., López, J., Rodríguez, A., García, J., … Molina, R. (2013). An intelligent computing technique to estimate the magnetic field generated by overhead transmission lines using a hybrid GA-Sx algorithm. *Internarional Journal of Electrical Power & Energy Systems, 53*, 43–53. https://doi.org/10.1016/J.IJEPES.2013.03.023

Nassiri, P., Monazzam, M., Hosseyni, S., Azam, K., & Shalkouhi, P. (2018). Extremely low-frequency electromagnetic field due to power substations in urban environment. *Environmental Engineering & Mangement Journal, 17*(8). https://doi.org/10.30638/eemj.2018.181.

Paniagua, J., Rufo, M., Jiménez, A., & Antolín, A. (2020). Dimensionless coefficients for assessing human exposure to radio-frequency electromagnetic fields indoors and outdoors in urban areas. *Environmental Research, 183*, Article 109188. https://doi.org/10.1016/j.envres.2020.109188

Rathebe, P., & Mbonane, T. (2018). Emission levels of ELF magnetic fields from 132 kV distribution substations. In *4th Global Electromagnetic Compatibility Conference (GEMCCON). Stellenbosch (South Africa)*. https://doi.org/10.1109/GEMCCON.2018.8628573

Rozov, V., Pelevin, D., & Pielievina, K. (2017). External magnetic field of urban transformer substation and methods of its normalization. *Electrical Engineering & Electromechanics, 5*, 60–66. https://doi.org/10.20998/2074-272X.2017.5.10.

Safigianni, A., & Tsompanidou, C. (2009). Electric and magnetic field measurements in an outdoor electric power substation. *IEEE Transactions on Power Delivery, 24*(1), 38–42. https://doi.org/10.1109/TPWRD.2008.917690

Saini, R., Roy, P. P., & Dogra, D. P. (2018). A segmental HMM based trajectory classification using genetic algorithm. *Expert Systems with Applications, 93*, 169–181. https://doi.org/10.1016/j.eswa.2017.10.021

Sato, K., & Fujii, T. (2017). Kriging-based interference power constraint: Integrated design of the radio environment map and transmission power. *IEEE Transactions on Cognitive Communications and Networking, 3*(1), 13–25. https://doi.org/10.1109/TCCN.2017.2653189

Sturman, V. (2019). Power frequency electromagnetic fields in the urban environment as the object of ecological-geographical research. *Geography and Natural Resources, 40*(1), 15–21. https://doi.org/10.1134/S1875372819010037

Tang, C., Yang, C., Cai, R., Ye, H., Duan, L., Zhang, Z., & Zhang, H. (2019). Analysis if the relationship between electromagnetic radiation characteristics and urban functions

in highly populated urban areas. *Science of the Total Environment, 654*, 535–540. https://doi.org/10.1016/j.scitotenv.2018.11.143

Zhang, S., Dai, S., Zanchettin, A., & Villa, R. (2020). Trajectory planning based on non-convex global optimization for serial manipulators. *Applied Mathematical Modelling, 84*, 89–105. https://doi.org/10.1016/j.apm.2020.03.004

Zhu, S., & Aksun-Guvenc, B. (2020). Trajectory planning of autonomous vehicles based on parameterized control optimization in dynamic on-road environments. *Journal of Intelligent & Robotic Systems, 100*(3), 1055–1067. https://doi.org/10.1007/s10846-020-01215-y